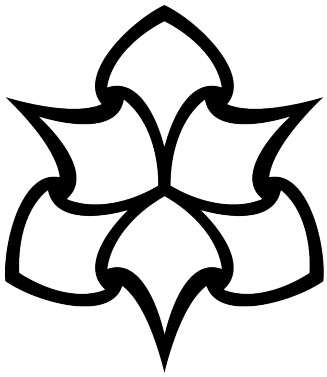

electronics

MDPI

Article

I/Q Imbalance and Imperfect SIC on Two-Way Relay NOMA Systems

Xinji Tian [1], Qianqian Li [1], Xingwang Li [1], Hongxing Peng [1,*], Changsen Zhang [1], Khaled M. Rabie [2,*] and Rupak Kharel [3]

[1] School of Physics and Electronic Information Engineering, Henan Polytechnic University, Jiaozuo 454003, China; tian215216@sohu.com (X.T.); liqianqian_lf@163.com (Q.L.); lixingwang@hpu.edu.cn (X.L.); zhangchangsen@hpu.edu.cn (C.Z.)

[2] Department of Engineering, Manchester Metropolitan University, Manchester M1 5GDM1 5GD, UK

[3] Department of Computing and Mathematics, Manchester Metropolitan University, Manchester M15 6BH, UK; R.Kharel@mmu.ac.uk

* Correspondence: phx@hpu.edu.cn (H.P.); K.Rabie@mmu.ac.uk (K.M.R.); Tel.: +1-560-931-0591 (K.M.R.)

Received: 24 December 2019; Accepted: 1 February 2020; Published: 3 February 2020

Abstract: Non-orthogonal multiple access (NOMA) system can meet the demands of ultra-high data rate, ultra-low latency, ultra-high reliability and massive connectivity of user devices (UE). However, the performance of the NOMA system may be deteriorated by the hardware impairments. In this paper, the joint effects of in-phase and quadrature-phase imbalance (IQI) and imperfect successive interference cancellation (ipSIC) on the performance of two-way relay cooperative NOMA (TWR C-NOMA) networks over the Rician fading channels are studied, where two users exchange information via a decode-and-forward (DF) relay. In order to evaluate the performance of the considered network, analytical expressions for the outage probability of the two users, as well as the overall system throughput are derived. To obtain more insights, the asymptotic outage performance in the high signal-to-noise ratio (SNR) region and the diversity order are analysed and discussed. Throughout the paper, Monte Carlo simulations are provided to verify the accuracy of our analysis. The results show that IQI and ipSIC have significant deleterious effects on the outage performance. It is also demonstrated that the outage behaviours of the conventional OMA approach are worse than those of NOMA. In addition, it is found that residual interference signals (IS) can result in error floors for the outage probability and zero diversity orders. Finally, the system throughput can be limited by IQI and ipSIC, and the system throughput converges to a fixed constant in the high SNR region.

Keywords: two-way relay; non-orthogonal multiple access; in-phase and quadrature-phase imbalance; imperfect successive interference cancellation; orthogonal multiple access

1. Introduction

The demand for new services and data rate has exploded for wireless communication, due to the growth of data traffic in the mobile Internet. To this end, a higher data rate and massive mobile terminal access are required for the 5th Generation (5G) systems [1–3]. Many new technologies such as massive multiple-input multiple-output (MIMO), non-orthogonal multiple access (NOMA), millimetre wave and device-to-device communication have been proposed to meet these demands [4]. Among these techniques, NOMA can significantly improve the spectral efficiency and reduce the system latency. Different from the conventional orthogonal multiple access (OMA), NOMA provides services for multiple users on the same resource by using superposition coding at the transmitter and successive interference cancellation (SIC) at the receiver [5,6]. Take an example of downlink: signals from the base station (BS) are superimposed and sent to NOMA users. Users with stronger channel gains decode

signals of other users with lower channel gains before decoding their own signals based on the SIC technique [7]. Hence, NOMA can support multiple users with limited resources and improve spectral efficiency, which has attracted considerable attention from academia and industry. For instance, in [8,9], the authors discussed power allocation under various criteria for a downlink NOMA system. In order to improve the system throughput, a network NOMA technique was proposed and analysed for the uplink coordinated multi-point transmission (CoMP) in [10].

Cooperative communications is another solution to mitigate the fading effects of wireless environments [11]. NOMA in cooperative communication systems is commonly referred to as cooperative-NOMA (C-NOMA), which is able to enhance the system reliability [12]. The authors analysed the effect of the power allocation coefficient on the error performance under a one-way relay C-NOMA system in [13]. The authors in [14] presented a new system detection scheme for a one-way relay C-NOMA system, which used the maximal ratio combining (MRC) and SIC to decode signals. Sheng Luo et al. in [15] proposed an adaptive transmission scheme based on a one-way relay C-NOMA network with a dedicated relay, which could temporarily store the received information. Recently, two-way relaying (TWR) has attracted a great deal of research attention because of its ability to achieve higher spectral efficiency in comparison to one-way relaying. It has advantages in the utilization of wireless networks' resources, improving spectral efficiency and enhancing network quality with regards to network throughput and error rate performance [16]. In [17], the authors proposed a scheme of jointly optimizing power and time allocations to minimize outage probability for a TWR C-NOMA network. To increase the system throughput and to ensure secure communications, the authors in [18] derived closed-form expressions of the ergodic secrecy rates under both non-colluding and colluding eavesdroppers in a TWR C-NOMA network. In order to achieve a balance between spectral efficiency and energy conservation, power allocation was discussed for a TWR C-NOMA system in [19].

According to the principle of NOMA, downlink users with stronger channel gains need to decode signals of other users with lower channel gains before decoding their own signals based on the SIC technique [20]. The NOMA systems with perfect SIC (pSIC) conditions were investigated in most of the above works, which is too idealistic. More in particular, the interference signals (IS) cannot be completely cancelled by SIC in practical applications [21]. In order to study the network with more practical scenarios, the imperfect SIC (ipSIC) condition was assumed for the NOMA system in many literature works. For instance, in [22], the outage probability was derived for NOMA systems with ipSIC in the underlay cognitive radio network. In order to maximize the sum rate for a NOMA network with ipSIC, the authors in [23] optimized the circularity coefficient of the improper Gaussian signalling (IGS) of the downlink NOMA system. Furthermore, Abu Mahady et al. [24] discussed a massive NOMA system in the presence of ipSIC and proposed several schemes to improve the overall system performance.

With the development of RF digital-to-analogue converters directly operating at the channel frequency, digital-intensive polar and quadrature TX architectures have received much attention [25]. The authors in [26] presented a novel digital-intensive hybrid transmitter (TX) architecture, combining conventional in-phase and quadrature (I/Q) with constrained phase modulation. However, it is well known that the RF transceivers of the hardware may not be perfect due to limitations of the technology in the actual communication scenario [27–29]. In practice, the hardware is damaged by the following: phase noise I/Q imbalance (IQI) and high power amplifier non-linearities [30–32]. In particular, some existing papers have studied the influence of hardware impairments of IQI on the system performance. In [27], a method of a non-iterative blind compensator to mitigate IQI was introduced and investigated by using inactive subcarriers in orthogonal frequency division multiplexing with index modulation (OFDM-IM) data transmission. To investigate the effect of different IQI on the channel estimation and sum rate, Kolomvakis et al. [33] derived the linear minimum mean square error estimator on a MIMO system with large antenna arrays. Furthermore, the expressions of the outage probability were derived by assuming that all the destinations and relay nodes were IQI impaired in [34].

Looking at the open up-to-date technical literature, most works used Rayleigh fading channel, which simplifies all mathematical operations widely. However, when a mirror or line-of-sight (LoS) component exists between the transmitter and the receiver, it cannot capture the change of fading. In addition, the future 5G wireless network will tend to a super-dense deployment, which will lead to more LoS transmissions due to the short propagation distance [35]. Therefore, it is very necessary to study NOMA systems with Rician fading channels [36].

1.1. Contributions

In this paper, we focus on a TWR C-NOMA system with one relay and two users. Two users wish to exchange information via the DF relay in two phases: the uplink multiple access process and the downlink broadcast process. It is worth mentioning that a more practical application scenario is considered in this paper. In other words, we analyse and discuss the performance of a TWR C-NOMA system with IQI and ipSIC conditions over the Rician fading channels. The main contributions of this work are summarized as follows:

- Based on the above works, we investigate the effects of IQI and ipSIC on the performance of a TWR C-NOMA network over the Rician fading channels. It is worth noting that this is a valuable problem for practical system design and analysis. As far as the authors know, although a system with IQI or ipSIC has been studied in some papers, the TWR C-NOMA system model with the condition of IQI and ipSIC under Rician fading channels has not been previously studied.
- We derive analytical expressions for outage probabilities of both the far and near users. The results show that IQI and ipSIC have deleterious effects on the outage performance and residual IS. In order to gain better insights into the system performance, we compare the outage performance of NOMA and OMA for both the far and near users, and the results show that the outage performance of NOMA is better than that of OMA. By comparing Rician and Rayleigh fading channel conditions, it is found that the throughput of our considered system with Rician or Rayleigh fading channels is almost the same in ideal conditions, and IQI and ipSIC have worse effects on the system throughput with Rayleigh fading channels than on Rician.
- We carry out the asymptotic analysis in the high SNR region. Furthermore, based on asymptotic outage probability, the diversity order is derived to analyse the diversity gain of the system. It is demonstrated that residual IS can result in error floors for the outage probability and zero diversity orders.

1.2. Organization

The rest of this paper is organized as follows. In Section 2, we describe the TWR C-NOMA system model in detail. In Section 3, the analytical and asymptotic been expressions of the outage probabilities, diversity order and the system throughput are obtained. Numerical examples of the derived analytical expressions and Monte Carlo simulations are given in Section 4. Finally, the conclusions are presented in Section 5.

1.3. Notations

In this paper, the main notations are shown as follows: $(\cdot)^*$ is the operator of the conjugate. The notation $f(x)$ represents the probability density function (PDF) of the independent variable x, while $F(x)$ represents the cumulative density function (CDF) of x. $E(\cdot)$ is the expectation operator. $\sum(\cdot)$ represents the operation of summation, and $I_0(\cdot)$ is the zeroth order modified Bessel function of the first kind. x^* represents the conjugation of x. $x \sim N\left(0, \sigma^2\right)$ represents that x follow Gaussian distributions. In addition, the list of acronyms used in this paper is listed in Table 1.

Table 1. Table of acronyms.

Acronyms	Definition
NOMA	Non-orthogonal multiple access
UE	User devices
OMA	Orthogonal multiple access
ipSIC	Imperfect successive interference cancellation
pSIC	Perfect successive interference cancellation
PDF	Probability density function
CDF	Cumulative density function
5G	5th Generation
TWR C-NOMA	Two-way relay cooperative NOMA
DF	Decode-and-forward
BS	Base station
COMP	Coordinated multi-point transmission
MRC	Maximal ratio combining
IGS	Improper Gaussian signalling
TX	Transmitter
RX	Receiver
IQI	In-phase and quadrature imbalance
OFDM-IM	Orthogonal frequency division multiplexing with index modulation
LoS	Line-of-sight
AWGN	Additive white Gaussian noise
SNR	Signal-to-noise ratio
SINR	Signal-to-interference plus noise ratio
IS	Interference signals
MIMO	Multiple-input multiple-output

2. System Model

We consider a TWR C-NOMA network over Rician fading channels as depicted in Figure 1, which consists of one relay R and a near user D_1 and a far user D_2. It was assumed that there is no direct link between D_1 and D_2 due to severe shadowing or obstacle. In this case, D_1 and D_2 can only communicate via a half-duplex (HD) DF relay. We also assumed that the two users and the relay were equipped with a single antenna. In this study, h_{RD_1} and h_{RD_2} are modelled as R to D_1 link and R to D_2 link, respectively.

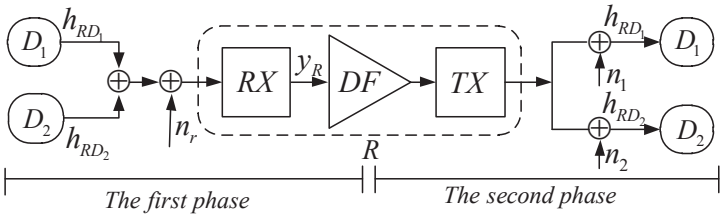

Figure 1. System model.

2.1. I/Q Imbalance Signal Model

Considering IQI at the transmitter (TX) [37], the time domain baseband signal can be obtained as:

$$\hat{s} = \mu_t s + \nu_t^* s^*, \tag{1}$$

where s and s^* denote the baseband IQI-free signal and the IQI impaired signal, respectively; μ_t and ν_t are the IQI coefficients; and ν_t^* is the conjugation of ν_t. As in [37], μ_t and ν_t are given as follows:

$$\mu_t \triangleq \frac{\left(1 + g_t e^{j\varphi_t}\right)}{2}, \tag{2}$$

$$\nu_t \triangleq \frac{\left(1 - g_t e^{-j\varphi_t}\right)}{2}, \tag{3}$$

where $g_t \sim N\left(0, \sigma_{g_t}^2\right)$ and $\varphi_t \sim N\left(0, \sigma_{\varphi_t}^2\right)$ are the TX amplitude and phase mismatch, respectively, which follow the Gaussian distribution. Similarly, the time domain baseband representation of the RX IQI impaired signal can be obtained as:

$$\hat{y} = \mu_r y + \nu_r y^*, \tag{4}$$

where y^* is referred to as the mirror signal introduced by the IQI. μ_t and ν_t are the IQI coefficients caused by RX, which can be expressed as:

$$\mu_r \triangleq \frac{\left(1 + g_r e^{-j\varphi_r}\right)}{2}, \tag{5}$$

$$\nu_r \triangleq \frac{\left(1 - g_r e^{j\varphi_r}\right)}{2}, \tag{6}$$

where $g_r \sim N\left(0, \sigma_{g_r}^2\right)$ and $\varphi_r \sim N\left(0, \sigma_{\varphi_r}^2\right)$ denote the RX amplitude and phase mismatch, respectively, which follow the Gaussian distribution. Therefore, the severity of TX IQI and RX IQI can be expressed as an image rejection ratio, which are defined as follows [38]:

$$IRR_T \triangleq \frac{|v_t|^2}{|\mu_t|^2}, \tag{7}$$

$$IRR_R \triangleq \frac{|v_r|^2}{|\mu_r|^2}, \tag{8}$$

2.2. Signal Model of Joint TX/RX Impaired by IQI

The whole communication process consists of two phases:

(1) The first time slot (up-link NOMA process): Two users send their signals to the relay. The relay receives the signals of the users with RX IQI, and the baseband received signal $\hat{y}_R$ at the relay is given by:

$$\hat{y}_R = \mu_r \left(h_{RD_1}\sqrt{a_1 P_u}s_1 + h_{RD_2}\sqrt{a_2 P_u}s_2\right) + \nu_r \left(h_{RD_1}^*\sqrt{a_1 P_u}s_1^* + h_{RD_2}^*\sqrt{a_2 P_u}s_2^*\right)^* + \mu_r n_r + \nu_r n_r^*, \tag{9}$$

where P_u denotes the total transmission power of the two users; $n_r \sim CN\left(0, N_0\right)$ is the additive white Gaussian noise (AWGN); a_1 and a_2 are the power allocation coefficients corresponding to D_1 and D_2 with $a_1 + a_2 = 1$ and $a_1 > a_2$, respectively.

The received signal-to-interference plus noise ratio (SINR) for the relay to decode the signal s_1 is given by:

$$\Gamma_{R \to s_1} = \frac{|\mu_r|^2 \rho_u \gamma_1 a_1}{|\nu_r|^2 \rho_u \gamma_1 a_1 + |A|^2 \rho_u \gamma_2 a_2 + |A|^2}, \tag{10}$$

where $\gamma_i \triangleq \left|h_{RD_i}\right|^2$, $|A|^2 = |\mu_r|^2 + |\nu_r|^2$ and $\rho_u = P_u / N_0$ denotes the transmit SNR at users.

It was assumed that the signal from D_1 can be correctly decoded at the relay. After eliminating s_1 by using SIC, the received SINR for the relay to decode the signal s_2 is expressed as:

$$\Gamma_{R \to s_2} = \frac{|\mu_r|^2 \rho_u \gamma_2 a_2}{|\nu_r|^2 \rho_u \gamma_1 a_1 + |\nu_r|^2 \rho_u \gamma_2 a_2 + \varepsilon |\mu_r|^2 \rho_u \gamma_1 a_1 + |A|^2}, \tag{11}$$

where $\varepsilon \in [0,1]$ is recorded as a parameter of ipSIC elimination and $\varepsilon = 0$ and $\varepsilon \neq 0$ denote pSIC and ipSIC, respectively.

(2) The second time slot (downlink NOMA process): The relay decodes the received signal and broadcasts the signals to the two users. The baseband received signals at D_1 with RX IQI denoted by $\hat{y}_{D_1}$ can be represented as:

$$\hat{y}_{D_1} = \mu_t h_{RD_1} \left(\mu_r \sqrt{b_1 P_r} s_1 + \mu_r \sqrt{b_2 P_r} s_2 \right) + \nu_t^* h_{RD_1} \left(\mu_r \sqrt{b_1 P_r} s_1 + \mu_r \sqrt{b_2 P_r} s_2 \right)^* + n_1, \tag{12}$$

where P_r denotes the transmission power at the relay. In addition, b_1 and b_2 are the responding power allocation coefficients for s_1 and s_2 with $b_1 + b_2 = 1$ and $b_1 > b_2$, respectively.

The baseband received signals at D_2 is given as:

$$\hat{y}_{D_2} = \mu_t h_{RD_2} \left(\mu_r \sqrt{b_1 P_r} s_1 + \mu_r \sqrt{b_2 P_r} s_2 \right) + \nu_t^* h_{RD_2} \left(\mu_r \sqrt{b_1 P_r} s_1 + \mu_r \sqrt{b_2 P_r} s_2 \right)^* + n_2, \tag{13}$$

where n_1 and n_2 are the AWGN at D_1 and D_2 with variance N_0, respectively.

It is assumed that neither D_1 nor D_2 know their own signals. The received SINR for D_1 to decode the signal s_1 is given by:

$$\Gamma_{D_1 \to s_1} = \frac{|\mu_t|^2 |\mu_r|^2 \rho_r \gamma_1 b_1}{\gamma_1 \left(|\nu_t^*|^2 |\mu_r|^2 \rho_r + |\mu_t|^2 |\mu_r|^2 \rho_r b_2 \right) + 1}, \tag{14}$$

where $\rho_r = P_r / N_0$ represents the transmit SNR at the users, and the received SINR for D_1 to decode s_2 is given by:

$$\Gamma_{D_1 \to s_2} = \frac{|\mu_t|^2 |\mu_r|^2 \rho_r \gamma_1 b_2}{\gamma_1 \left(\varepsilon |\mu_t|^2 |\mu_r|^2 \rho_r b_1 + |\nu_t^*|^2 |\mu_r|^2 \rho_r \right) + 1}. \tag{15}$$

The received SINR for D_2 to decode the signal s_1 is given by:

$$\Gamma_{D_2 \to s_1} = \frac{|\mu_t|^2 |\mu_r|^2 \rho_r \gamma_2 b_1}{\gamma_2 \left(|\mu_t|^2 |\mu_r|^2 \rho_r b_2 + |\nu_t^*|^2 |\mu_r|^2 \rho_r \right) + 1}. \tag{16}$$

The PDF of the random variable γ_i is expressed as [39]:

$$f_{\gamma_i}(x) = \frac{(K+1) e^{-K}}{\lambda_i} e^{-\frac{(K+1)}{\lambda_i} x} I_0 \left(2 \sqrt{\frac{K(K+1)x}{\lambda_i}} \right), \tag{17}$$

where λ_i is the mean value of γ_i, $i = 1, 2$. K is the Rician fading parameter, which represents the ratio of the power of the LoS component to the average power of the non-LoS component. $I_0(\cdot)$ is the zeroth order modified Bessel function of the first kind.

Applying the result of [39], the PDF of λ_i can be rewritten as follows:

$$f_{\gamma_i}(x) = \bar{a}_i \sum_{l=0}^{\infty} \frac{\left(\bar{b}_i K \right)^l}{(l!)^2} x^l e^{-\bar{b}_i x}, \tag{18}$$

where $\bar{a}_i = (K+1) e^{-K} \lambda_i^{-1}$, $\bar{b}_i = (K+1) \lambda_i^{-1}$ and $I_0(x) = \sum_{l=0}^{\infty} x^{2l} 2^{-2l} (l!)^{-2}$. Based on this, the CDF of γ_i is:

$$F_{\gamma_i}(\varsigma) = \int_0^{\varsigma} f_{\gamma_i}(x) \, dx = 1 - \frac{\bar{a}_i}{\bar{b}_i} \sum_{l=0}^{\infty} \sum_{m=0}^{l} \frac{K^l \bar{b}_i^m}{l! m!} \varsigma^m e^{-\bar{b}_i \varsigma}. \tag{19}$$

3. Performance Analysis

In this section, we derive analytical expressions for the outage probability of the system under consideration. The asymptotic outage behaviour and diversity orders are also discussed. Then, the system throughput is obtained.

3.1. Outage Probability Analysis

The outage probabilities for the $D_1 \to R \to D_2$ link and the $D_2 \to R \to D_1$ link are denoted by P_{out,D_1} and P_{out,D_2}, respectively.

The outage event of P_{out,D_1} occurs in the following cases: (1) the information s_1 cannot be decoded by R; (2) the information s_1 cannot be decoded by D_2. Thus, the outage probability of D_1 can be written as:

$$\mathrm{P}_{out,D_1} = 1 - \Pr\left(\Gamma_{R\to s_1} > \gamma_{thf}\right) \Pr\left(\Gamma_{D_2\to s_1} > \gamma_{thf}\right). \tag{20}$$

In addition, the outage event of P_{out,D_2} occurs in the following cases: (1) s_1 cannot be decoded by R correctly. (2) s_2 cannot be decoded by R after R can first decode s_1 correctly. (3) s_1 cannot be decoded by D_1 correctly. (4) s_2 cannot be decoded by D_1, while D_1 can first decode s_1 correctly. Thus, the outage probability of D_2 can be written as:

$$\mathrm{P}_{out,D_2} = 1 - \Pr\left(\Gamma_{R\to s_1} > \gamma_{thf}, \Gamma_{R\to s_2} > \gamma_{thm}\right) \Pr\left(\Gamma_{D_1\to s_1} > \gamma_{thm}, \Gamma_{D_1\to s_2} > \gamma_{thm}\right), \tag{21}$$

where $\gamma_{thf} = 2^{\bar{R}_1} - 1$ and $\gamma_{thm} = 2^{\bar{R}_2} - 1$, with $\bar{R}_1$ and $\bar{R}_2$ denoting the data rate thresholds for users D_1 and D_2, respectively.

Theorem 1. The analytical expression of the outage probability of D_1 for the TWR C-NOMA network with IQI and ipSIC can be obtained as:

$$\begin{aligned}\mathrm{P}_{out,D_1}^{IQI,ipSIC} = 1 - \sum_{l_3=0}^{\infty}\sum_{m_3=0}^{l_3} &\frac{\Theta_1\,(n+j)!K^{l_3}\bar{a}_2\bar{b}_2^{m_3-1}}{l_3!m_3!\left(|A|^2\bar{b}_1\beta_f a_2\rho_u + \bar{b}_2\right)^{(n+j+1)}} \\ &\times \left(\frac{\gamma_{thf}}{|\mu_r|^2\rho_r b_1\left(|\mu_t|^2 - \gamma_{thf}|\nu_t^*|^2\right)}\right)^{m_3} e^{-\frac{\bar{b}_2\gamma_{thf}}{|\mu_r|^2\rho_r b_1\left(|\mu_t|^2-\gamma_{thf}|\nu_t^*|^2\right)}},\end{aligned} \tag{22}$$

where $\Theta_1 = \sum_{j=0}^{\infty}\sum_{l=0}^{\infty}\sum_{m=0}^{l}\sum_{n=0}^{m}\binom{m}{n}\beta_0\beta_f^m\left(|A|^2\right)^m a_2^n\rho_u^n e^{-\bar{b}_1\beta_f|A|^2}$ *with* $\beta_0 = \frac{\bar{a}_1\bar{a}_2K^{l+j}\bar{b}_1^{m-1}\bar{b}_2^{j}}{(j!)^2 l!m!}$ *and* $\beta_f = \frac{\gamma_{thf}}{\rho_u a_1\left(|\mu_r|^2-\gamma_{thf}|\nu_r|^2\right)}$ *with* $|\mu_t|^2 > \gamma_{thf}|\nu_t^*|^2$.

Proof. Please see Appendix A. □

Theorem 2. The analytical expression of the outage probability of D_2 for the TWR C-NOMA network with IQI and ipSIC can be obtained as:

$$\begin{aligned}\mathrm{P}_{out,D_2}^{IQI,ipSIC} = 1 - \sum_{l_2=0}^{\infty}\sum_{m_2=0}^{l_2} &\frac{\Theta_1\Theta_2\,(n+j)!\,(j_1+n_1)!}{l_2!m_2!\left(|A|^2\bar{b}_1\beta_f a_2\rho_u + \bar{b}_2\right)^{(n+j+1)}} \\ &\times \frac{K^{l_2}\bar{a}_1\bar{b}_1^{m_2-1}\beta_0^{m_2}e^{-\bar{b}_1\beta_0}}{\left(\bar{b}_2\beta_m a_1\rho_u\left(|\nu_r|^2 + \varepsilon|\mu_r|^2\right) + \bar{b}_1\right)^{(j_1+n_1+1)}},\end{aligned} \tag{23}$$

where $\Theta_2 = \sum_{j_1=0}^{\infty}\sum_{l_1=0}^{\infty}\sum_{m_1=0}^{l_1}\sum_{n_1=0}^{m_1}\binom{m_1}{n_1}\frac{\bar{a}_1\bar{a}_2K^{l_1+j_1}\Theta_3}{(j_1!)^2 l_1! m_1!}e^{-\bar{b}_2\beta_m|A|^2}$; $\beta_m = \frac{\gamma_{thm}}{\rho_u a_2\left(|\mu_r|^2-\gamma_{thm}|\nu_r|^2\right)}$, *with* $|\mu_r|^2 > \gamma_{thm}|\nu_r|^2$; $\Theta_3 = \bar{b}_2^{m_1-1}\bar{b}_1^{j_1}\beta_m^{m_1}a_1^{n_1}\rho_u^{n_1}\left(|\nu_r|^2+\varepsilon|\mu_r|^2\right)^{n_1}\left(|A|^2\right)^{m_1-n_1}$; $\beta_0 = \max(\beta_1,\beta_2)$; $\beta_2 = \frac{\gamma_{thm}}{|\mu_r|^2\rho_r\left(|\mu_t|^2 b_2-\gamma_{thm}\left(\varepsilon|\mu_t|^2 b_1+|\nu_t^*|^2\right)\right)}$, *with* $\varepsilon = [0,1]$, $b_2 > \frac{\gamma_{thm}\left(\varepsilon|\mu_t|^2 b_1+|\nu_t^*|^2\right)}{|\mu_t|^2}$ *and* $\beta_1 = \frac{\gamma_{thf}}{|\mu_r|^2\rho_r\left(|\mu_t|^2 b_1-\gamma_{thf}\left(|\nu_t^*|^2+|\mu_t|^2 b_2\right)\right)}$, *with* $b_1 > \frac{\gamma_{thf}\left(|\nu_t^*|^2+|\mu_t|^2 b_2\right)}{|\mu_t|^2}$.

Proof. Please see Appendix B. □

3.2. Asymptotic Outage Probability Analysis

To get more insight into the outage behaviour of the TWR C-NOMA system with IQI and ipSIC, the formulas of asymptotic outage probabilities at the high SNR region are derived in this subsection.

Proposition 1. Based on (22), when $\rho_u = \varsigma\rho_r \to \infty$ and $\varsigma > 0$, the asymptotic outage probability of D_1 is derived as:

$$\mathrm{P}_{out,D_1}^{\infty,IQI,ipSIC} = 1 - \sum_{l_3=0}^{\infty}\sum_{j=0}^{\infty}\sum_{l=0}^{\infty}\sum_{m=0}^{l}\frac{\bar{a}_1\bar{a}_2^2K^{l+j+l_3}\bar{b}_1^{m-1}\bar{b}_2^{j-1}\left(\beta'_f\right)^m\left(|A|^2\right)^m a_2^m(m+j)!}{(j!)^2 l!m!l_3!\left(|A|^2\bar{b}_1\beta'_f a_2+\bar{b}_2\right)^{(m+j+1)}}, \tag{24}$$

where $\beta'_f = \frac{\gamma_{thf}}{a_1\left(|\mu_r|^2-\gamma_{thf}|\nu_r|^2\right)}$, *with* $|\mu_r|^2 > \gamma_{thf}|\nu_r|^2$.

Proposition 2. Based on (23), when $\rho_u = \varsigma\rho_r \to \infty$ and $\varsigma > 0$, the asymptotic outage probability of D_2 is given by:

$$\begin{aligned}\mathrm{P}_{out,D_2}^{\infty,IQI,ipSIC} = 1 &- \sum_{l_2=0}^{\infty}\sum_{m_2=0}^{l_2}\frac{\Phi_1\Phi_2(n+j)!(j_1+n_1)!}{l_2!m_2!\left(|A|^2\bar{b}_1\beta'_f a_2+\bar{b}_2\right)^{(n+j+1)}}\\ &\times\frac{K^{l_2}\bar{a}_1\left(\bar{b}_1\right)^{m_2-1}\left(\beta'_0\right)^{m_2}e^{-\bar{b}_1\beta'_0}}{\left(\bar{b}_2\beta'_m a_1\left(|\nu_r|^2+\varepsilon|\mu_r|^2\right)+\bar{b}_1\right)^{(j_1+n_1+1)}},\end{aligned} \tag{25}$$

where $\Phi_2 = \sum_{j_1=0}^{\infty}\sum_{l_1=0}^{\infty}\sum_{m_1=0}^{l_1}\frac{\bar{a}_1\bar{a}_2K^{l_1+j_1}\bar{b}_2^{m_1-1}\bar{b}_1^{j_1}}{(j_1!)^2 l_1! m_1!}$, $\Phi_3 = \left(\beta'_m\right)^{m_1}a_1^{m_1}\left(|\nu_r|^2+\varepsilon|\mu_r|^2\right)^{m_1}$, $\beta'_m = \frac{\gamma_{thm}}{a_2\left(|\mu_r|^2-\gamma_{thm}|\nu_r|^2\right)}$ *with* $|\mu_r|^2 > \gamma_{thm}|\nu_r|^2$ *and* $\Phi_1 = \sum_{j=0}^{\infty}\sum_{l=0}^{\infty}\sum_{m=0}^{l}\frac{\bar{a}_1\bar{a}_2K^{l+j}\bar{b}_1^{m-1}\bar{b}_2^{j}\left(\beta'_f\right)^m\left(|A|^2\right)^m a_2^n}{(j!)^2 l!m!}$.

3.3. Diversity Orders

In this subsection, the diversity order is analysed, which is defined as [16]:

$$d = -\lim_{\rho\to\infty}\frac{\log\left(\mathrm{P}_{D_n}^{\infty}(\rho)\right)}{\log\rho}, \tag{26}$$

where $\rho = \rho_u = \varsigma\rho_r$ and $\mathrm{P}_{D_n}^{\infty}$ denotes the asymptotic outage probability of D_n, $n = 1,2$.

By using the definition in (26), the diversity orders for the IQI and ipSIC conditions of both D_1 and D_2 are respectively derived as follows:

$$d_{D_1}^{IQI,ipSIC} = -\lim_{\rho\to\infty} \frac{\log\left(\mathrm{P}_{out,D_1}^{\infty,IQI,ipSIC}(\rho)\right)}{\log\rho} = 0, \tag{27}$$

$$d_{D_2}^{IQI,ipSIC} = -\lim_{\rho\to\infty} \frac{\log\left(\mathrm{P}_{out,D_2}^{\infty,IQI,ipSIC}(\rho)\right)}{\log\rho} = 0. \tag{28}$$

The diversity orders of both D_1 and D_2 for the considered system with the ideal condition (I/Q balance and pSIC) are derived as:

$$d_{D_1}^{ideal} = -\lim_{\rho\to\infty} \frac{\log\left(\mathrm{P}_{out,D_1}^{\infty,ideal}(\rho)\right)}{\log\rho} = 0, \tag{29}$$

$$d_{D_2}^{ideal} = -\lim_{\rho\to\infty} \frac{\log\left(\mathrm{P}_{out,D_2}^{\infty,ideal}(\rho)\right)}{\log\rho} = 0. \tag{30}$$

Remark 1. *An important conclusion from the analysis above is that due to the impact of IQI and residual interference with the use of ipSIC, the diversity orders of D_1 and D_2 are both zero due to the fixed outage probabilities at the high SNR region. As can be observed, there are error floors for D_1 and D_2 with IQI and ipSIC.*

3.4. System Throughput Analysis

In order to further evaluate the performance of the TWR C-NOMA system, the system throughput is obtained for IQI and ipSIC conditions, as well as for that of the ideal condition, respectively, and given by:

$$R^{IQI,ipSIC} = \left(1 - \mathrm{P}_{out,D_1}^{IQI,ipSIC}\right)\bar{R}_1 + \left(1 - \mathrm{P}_{out,D_2}^{IQI,ipSIC}\right)\bar{R}_2, \tag{31}$$

$$R^{ideal} = \left(1 - \mathrm{P}_{out,D_1}^{ideal}\right)\bar{R}_1 + \left(1 - \mathrm{P}_{out,D_2}^{ideal}\right)\bar{R}_2, \tag{32}$$

where $\bar{R}_1$ and $\bar{R}_2$ represent the target rates at the receiver to decode the desired signals s_1 and s_2, respectively.

4. Numerical Examples and Discussions

In this section, we provide numerical illustration of our analytical results through Monte Carlo simulations. Unless otherwise specified, the main parameter values used in all our evaluations are provided in Table 2.

Table 2. Table of parameters used for numerical results.

Monte Carlo Simulations Repeated	**10^5 Iterations**
Power allocation coefficients of NOMA	$a_1 = 0.7$, $a_2 = 0.3$, $b_1 = 0.8$ and $b_2 = 0.2$
Targeted data rates	$\bar{R}_1 = 0.2BPCU$, $\bar{R}_2 = 0.3BPCU$
The distance between R and D_1 or D_2	$d_1 = 0.5$, $d_2 = 1$
Noise power	$N_0 = 1$
The parameters of ipSIC	$\varepsilon = 0.03$
Ideal RF front end	$g_t = g_r = 1$, $\varphi_t = \varphi_r = 0^\circ$
The parameters of IQI	$g_t = g_r = 0.8$, $\varphi_t = \varphi_r = 5^\circ$

Figure 2 plots the outage probabilities of two users versus transmit SNR with different conditions. The analytical curves for the outage probabilities of the IQI and ipSIC are plotted using (22) and (23). An excellent agreement can be observed between the analytical results and Monte Carlo simulations. We considered five conditions in this simulation: (1) IQI and ipSIC; (2) ONLY ipSIC; (3) NO-IQI and pSIC; (4) OMA; (5) Rayleigh fading channels. In addition, the asymptotic outage probability curves are plotted in accordance using (24) and (25). It is noticed from Figure 2 that the error floors exist for both D_1 and D_2. The reason is that the IS result in zero diversity order. The outage performance of the system with IQI is worse than that of the system without IQI, which means that IQI has deleterious effects on the system outage performance. Moreover, the outage performance of D_2 with ipSIC is worse than that of the system with pSIC, due to the residual interference caused by ipSIC. It can be seen that the outage performances of D_1 and D_2 for OMA are lower than NOMA. It is also interesting to note that the outage probability of D_1 with ipSIC or with pSIC has the same curves. This is due to the fact that the SIC method is not used in the decoding of the signal of D_1, which is proven by (22). Therefore, the outage performance of the Rayleigh condition is better than the Rician in D_1, and it is worse than the Rician condition in D_2.

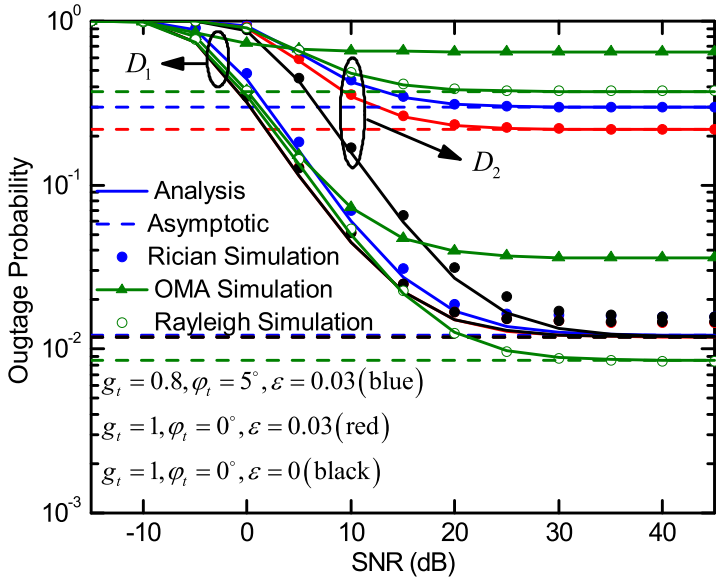

Figure 2. Outage probability versus the transmit SNR of the proposed TWR C-NOMA system for D_1 and D_2 with data rate thresholds $\bar{R}_1 = 0.2BPCU$ and $\bar{R}_2 = 0.3BPCU$.

Figure 3 plots the outage probabilities of the two users versus the parameter of ipSIC for the system with IQI and ideal conditions. It is clearly seen that the outage performance of D_2 becomes worse with the increase of ipSIC parameter. This is because the residual interference caused by ipSIC is harmful to the outage performance of D_2. In addition, the parameter of ipSIC has no effect on the outage probability of D_1, which is proven by (22). Finally, the outage performances for both D_1 and

D_2 with IQI are worse than that obtained without IQI condition. All in all, IQI reduces the system outage performance.

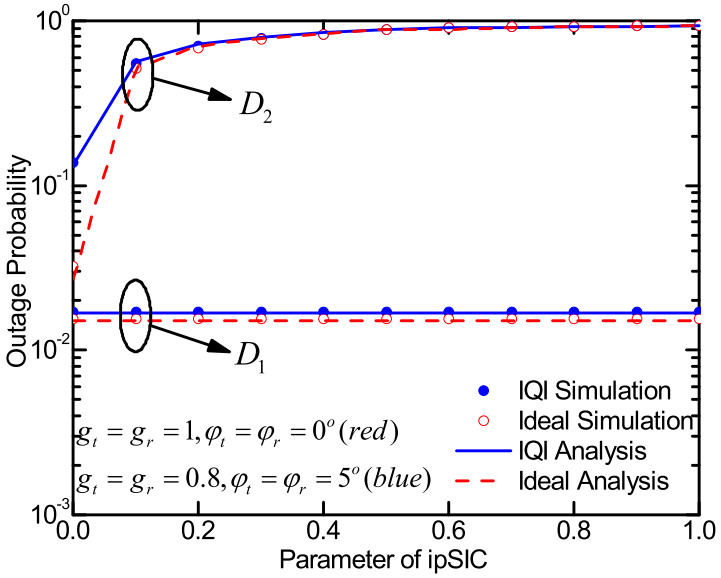

Figure 3. Outage probability versus the parameter of ipSIC for the system with IQI and ideal conditions.

In Figure 4, we show the outage probabilities of D_1 and D_2 with ipSIC under the different levels of phase mismatch. The outage performances of D_1 and D_2 deteriorate with the increase of the value of phase mismatch. The greater the gap between the value of the phase mismatch and zero degrees, the greater the adverse effect of the phase mismatch on outage performance.

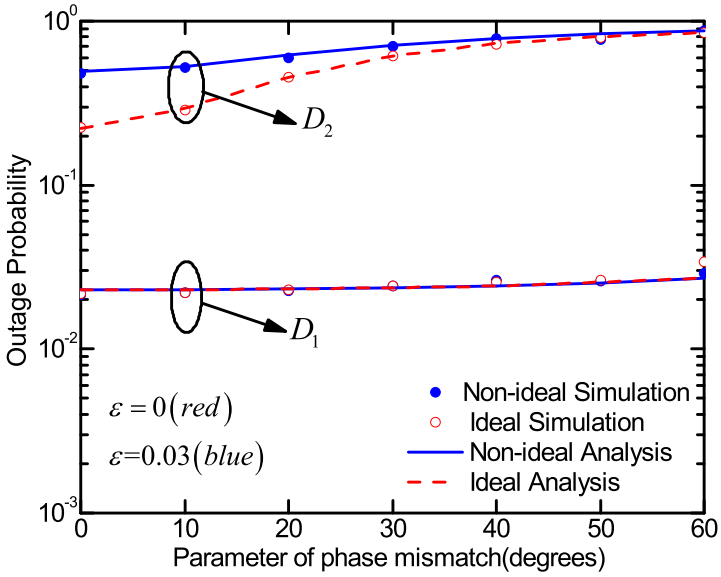

Figure 4. Outage probability versus the parameter of phase mismatch for the system with ipSIC and pSIC conditions.

Figure 5 plots the outage probabilities of the two users with respect to the amplitude mismatch with ipSIC and pSIC conditions. It is clearly seen that the closer the amplitude mismatch parameter is to one, the better the outage performance of D_1 and D_2 becomes. The greater the gap between the value of the amplitude mismatch and one, the greater the harmful effect of the amplitude mismatch on system performance.

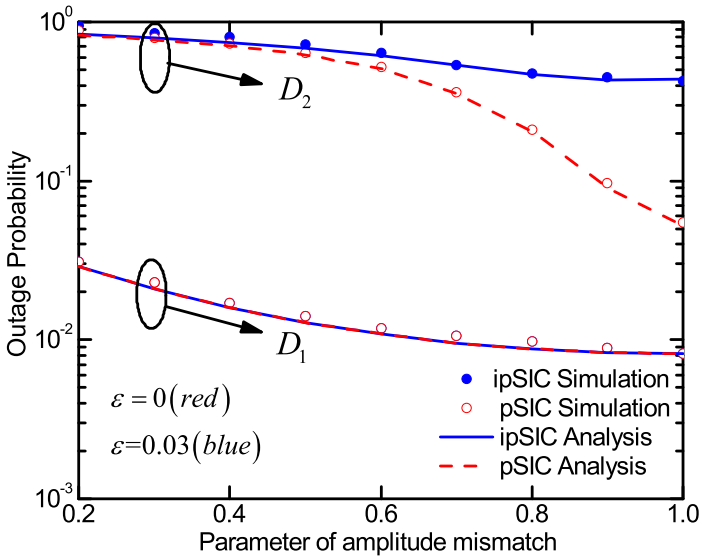

Figure 5. Outage probability versus the amplitude mismatch for the system with ipSIC and pSIC conditions.

The effects of the three different conditions for the system throughput are evaluated in Figure 6, in which we fix the parameters of IQI as $g_t = g_r = 0.8$, $\varphi_t = \varphi_r = 5^\circ$ and the ipSIC parameters as $\varepsilon = 0.03$ for the IQI and ipSIC conditions. For only the ipSIC condition, we fix the parameters of IQI as $g_t = g_r = 1$, $\varphi_t = \varphi_r = 0^\circ$ and ipSIC parameters as $\varepsilon = 0.03$. For the ideal condition, we use the parameters of IQI as $g_t = g_r = 1$, $\varphi_t = \varphi_r = 0^\circ$ and ipSIC parameters as $\varepsilon = 0$. In the SNR range from -10dB to 45dB, the analysis curves of the system throughput with IQI and/or ipSIC condition is always lower than that of the ideal condition. It should be noted that the system throughput enhances as the SNR increase. Moreover, both system throughputs gradually tend to be stable in high SNR region. It can be observed from Figure 6 that the system throughput under two channels is the same in the low SNR region, and at high SNRs, the Rayleigh fading is slightly better than the throughput of the Rician fading channels in the ideal condition. However, in other non-ideal conditions, it is obviously worse than Rician fading channels. Therefore, a conclusion can be obtained that there is almost no difference of the considered system throughput with the ideal condition in the two channel cases, and IQI and ipSIC have worse effects on the system throughput with Rayleigh fading channels than on Rician.

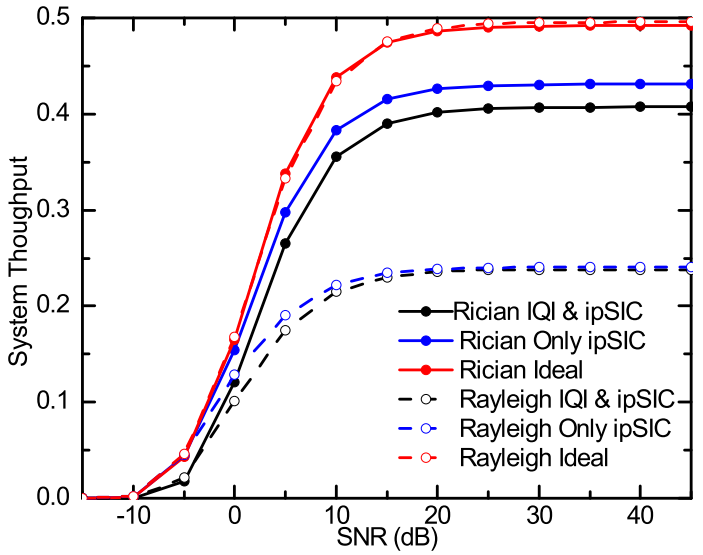

Figure 6. System throughput versus the transmit SNR of the proposed TWR C-NOMA system for D_1 and D_2 with data rate thresholds $\bar{R}_1 = 0.2BPCU$ and $\bar{R}_2 = 0.3BPCU$.

5. Conclusions

In this paper, the performance of a TWR C-NOMA system with IQI and ipSIC over the Rician fading channels was investigated. The analytical expressions of these performance metrics were obtained. In addition, the asymptotic outage behaviour and the diversity order were discussed in the high SNR region. Based on the analytical results, it was shown that the outage performance of the NOMA based system was better than that of OMA. The results revealed that the system outage performance could significantly deteriorate by the IQI and ipSIC. It was also presented that the IS resulted in a zero diversity order in the system. Moreover, the system throughput was found to improve with the increase of SNR, in which it converged to a fixed constant in the high SNR region.

Author Contributions: Conceptualization, X.L., Q.L., C.Z. and X.T.; data curation, X.L. and Q.L.; methodology, X.T., X.L. and Q.L.; software, Q.L.; supervision, X.T., H.P. and H.C.; validation, X.T., X.L., H.P., H.C., K.M.R. and R.K.; formal analysis, X.L., Q.L.; investigation, H.P., H.C., K.M.R. and R.K.; writing, original draft preparation, X.T. and Q.L.; writing, review and editing, X.L., Q.L., K.M.R. and R.K. All authors have read and agreed to the published version of the manuscript.

Funding: This work was supported in part by the Henan Scientific and Technological Research Project under Grant 182102210307, in part by the Fundamental Research Funds for the Universities of Henan Province under Grant NSFRF180309, in part by the Outstanding Youth Science Foundation of Henan Polytechnic University under Grant J2019-4, in part by the Key Scientific Research Projects of Higher Education Institutions in Henan Province under Grant 20A510007.

Conflicts of Interest: The authors declare no conflict of interest.

Appendix A. Proof of Theorem 1

Proof: According to (20), the outage probability for D_1 with ipSIC under the IQI condition is given by:

$$\begin{aligned} \mathrm{P}_{out,D_2}^{IQI,ipSIC} &= 1-\Pr\left(\Gamma_{R\to s_1}>\gamma_{thf}\right)\Pr\left(\Gamma_{D_2\to s_1}>\gamma_{thf}\right) \\ &= 1-\underbrace{\Pr\left(\frac{|\mu_r|^2\rho_u\gamma_1a_1}{|\nu_r|^2\rho_u\gamma_1a_1+|A|^2\rho_u\gamma_2a_2+|A|^2}>\gamma_{thf}\right)}_{f_1}\underbrace{\Pr\left(\frac{|\mu_t|^2|\mu_r|^2\rho_rb_1\gamma_2}{\gamma_2|\nu_t^*|^2|\mu_r|^2\rho_rb_1+1}>\gamma_{thf}\right)}_{f_2}, \end{aligned} \tag{A1}$$

$$\begin{aligned} f_1 &= \Pr\left(\frac{|\mu_r|^2\rho_u\gamma_1a_1}{|\nu_r|^2\rho_u\gamma_1a_1+|A|^2\rho_u\gamma_2a_2+|A|^2}>\gamma_{thf}\right) \\ &= \int_0^\infty f_{\gamma_2}(x)\frac{\bar{a}_1}{\bar{b}_1}\sum_{l=0}^{\infty}\sum_{m=0}^{l}\frac{K^l\bar{b}_1^m}{l!m!}\left(\beta_f\left(a_2|A|^2\rho_ux+|A|^2\right)\right)^m e^{-\bar{b}_1\beta_f\left(a_2|A|^2\rho_ux+|A|^2\right)}dx \end{aligned} \tag{A2}$$

$$= \frac{\Theta_1(n+j)!}{\left(|A|^2\bar{b}_1\beta_fa_2\rho_u+\bar{b}_2\right)^{(n+j+1)}}, \tag{A3}$$

where $\Theta_1=\sum_{j=0}^{\infty}\sum_{l=0}^{\infty}\sum_{m=0}^{l}\sum_{n=0}^{m}\binom{m}{n}\beta_0\beta_f^m\left(|A|^2\right)^m a_2^n\rho_u^n e^{-\bar{b}_1\beta_f|A|^2}$ with $\beta_0=\frac{\bar{a}_1\bar{a}_2K^{l+j}\bar{b}_1^{m-1}\bar{b}_2^j}{(j!)^2l!m!}$ and $\beta_f=\frac{\gamma_{thf}}{\rho_ua_1\left(|\mu_r|^2-\gamma_{thf}|\nu_r|^2\right)}$ with $|\mu_t|^2>\gamma_{thf}|\nu_t^*|^2$.

$$\begin{aligned} f_2 &= \Pr\left(\frac{|\mu_t|^2|\mu_r|^2\rho_rb_1\gamma_2}{\gamma_2|\nu_t^*|^2|\mu_r|^2\rho_rb_1+1}>\gamma_{thf}\right) \\ &= \sum_{l_3=0}^{\infty}\sum_{m_3=0}^{l_3}\frac{K^{l_3}\bar{a}_2\bar{b}_2^{m_3-1}}{l_3!m_3!}\left(\frac{\gamma_{thf}}{|\mu_r|^2\rho_rb_1\left(|\mu_t|^2-\gamma_{thf}|\nu_t^*|^2\right)}\right)^{m_3}e^{-\frac{\bar{b}_2\gamma_{thf}}{|\mu_r|^2\rho_rb_1\left(|\mu_t|^2-\gamma_{thf}|\nu_t^*|^2\right)}}, \end{aligned} \tag{A4}$$

Substituting (A3) and (A4) into (A1), (22) can be obtained in Theorem 1.

The proof is completed.

Appendix B. Proof of Theorem 2

Proof: According to (21), the outage probability for D_2 with ipSIC under IQI condition is given by:

$$\begin{aligned}
\mathrm{P}_{out,D_2}^{IQI,ipSIC} &= 1-\Pr\left(\Gamma_{R\to s_1}>\gamma_{thf},\Gamma_{R\to s_2}>\gamma_{thm}\right)\Pr\left(\Gamma_{D_1\to s_1}>\gamma_{thm},\Gamma_{D_1\to s_2}>\gamma_{thm}\right)\\
&=\underbrace{1-\Pr\left(\frac{|\mu_r|^2\rho_u\gamma_1 a_1}{|\nu_r|^2\rho_u\gamma_1 a_1+|A|^2\rho_u\gamma_2 a_2+|A|^2}>\gamma_{thf},\frac{|\mu_r|^2\rho_u\gamma_2 a_2}{\left(|\nu_r|^2+\varepsilon|\mu_r|^2\right)\rho_u\gamma_1 a_1+|\nu_r|^2\rho_u\gamma_2 a_2+|A|^2}>\gamma_{thm}\right)}_{f_3}\\
&\times\underbrace{\Pr\left(\frac{|\mu_t|^2|\mu_r|^2\rho_r\gamma_1 b_1}{\gamma_1\left(|\nu_t^*|^2|\mu_r|^2\rho_r+|\mu_t|^2|\mu_r|^2\rho_r b_2\right)+1}>\gamma_{thf},\frac{|\mu_t|^2|\mu_r|^2\rho_r\gamma_1 b_2}{\gamma_1\left(\varepsilon|\mu_t|^2|\mu_r|^2\rho_r b_1+|\nu_t^*|^2|\mu_r|^2\rho_r\right)+1}>\gamma_{thm}\right)}_{f_4},
\end{aligned}\tag{A5}$$

Therein, f_3 and f_4 can be rewritten as follows:

$$\begin{aligned}
f_3&=\Pr\left(\gamma_1>\beta_f\left(a_2|A|^2\rho_u\gamma_2+|A|^2\right),\gamma_2>\beta_m\left(a_1\rho_u\gamma_1\left(|\nu_r|^2+\varepsilon|\mu_r|^2\right)+|A|^2\right)\right)\\
&=\frac{\Theta_1\Theta_2\,(n+j)!\,(j_1+n_1)!}{\left(|A|^2\bar{b}_1\beta_f a_2\rho_u+\bar{b}_2\right)^{(n+j+1)}\left(\bar{b}_2\beta_m a_1\rho_u\left(|\nu_r|^2+\varepsilon|\mu_r|^2\right)+\bar{b}_1\right)^{(j_1+n_1+1)}},
\end{aligned}\tag{A6}$$

where $\Theta_2=\sum_{j_1=0}^{\infty}\sum_{l_1=0}^{\infty}\sum_{m_1=0}^{l_1}\sum_{n_1=0}^{m_1}\binom{m_1}{n_1}\frac{\bar{a}_1\bar{a}_2K^{l_1+j_1}\Theta_3}{(j_1!)^2 l_1!m_1!}e^{-\bar{b}_2\beta_m|A|^2}$; $\beta_m=\frac{\gamma_{thm}}{\rho_u a_2\left(|\mu_r|^2-\gamma_{thm}|\nu_r|^2\right)}$, with $|\mu_r|^2>\gamma_{thm}|\nu_r|^2$; $\Theta_3=\bar{b}_2^{m_1-1}\bar{b}_1^{j_1}\beta_m^{m_1}a_1^{n_1}\rho_u^{n_1}\left(|\nu_r|^2+\varepsilon|\mu_r|^2\right)^{n_1}\left(|A|^2\right)^{m_1-n_1}$.

$$\begin{aligned}
f_4&=\Pr\left(\frac{|\mu_t|^2|\mu_r|^2\rho_r\gamma_1 b_1}{\gamma_1\left(|\nu_t^*|^2|\mu_r|^2\rho_r+|\mu_t|^2|\mu_r|^2\rho_r b_2\right)+1}>\gamma_{thf},\frac{|\mu_t|^2|\mu_r|^2\rho_r\gamma_1 b_2}{\gamma_1\left(\varepsilon|\mu_t|^2|\mu_r|^2\rho_r b_1+|\nu_t^*|^2|\mu_r|^2\rho_r\right)+1}>\gamma_{thm}\right)\\
&=\Pr\left(\gamma_1>\beta_0=\max\left(\beta_1,\beta_2\right)\right)\\
&=\frac{\bar{a}_1}{\bar{b}_1}\sum_{l_2=0}^{\infty}\sum_{m_2=0}^{l_2}\frac{K^{l_2}\bar{b}_1^{m_2}}{l_2!m_2!}\beta_0^{m_2}e^{-\bar{b}_1\beta_0}.
\end{aligned}\tag{A7}$$

where $\beta_0=\max\left(\beta_1,\beta_2\right)$; $\beta_2=\frac{\gamma_{thm}}{|\mu_r|^2\rho_r\left(|\mu_t|^2b_2-\gamma_{thm}\left(\varepsilon|\mu_t|^2b_1+\left|\nu_t^*\right|^2\right)\right)}$, with $\varepsilon=[0,1]$, $b_2>\frac{\gamma_{thm}\left(\varepsilon|\mu_t|^2b_1+|\nu_t^*|^2\right)}{|\mu_t|^2}$ and $\beta_1=\frac{\gamma_{thf}}{|\mu_r|^2\rho_r\left(|\mu_t|^2b_1-\gamma_{thf}\left(\left|\nu_t^*\right|^2+|\mu_t|^2b_2\right)\right)}$, with $b_1>\frac{\gamma_{thf}\left(|\nu_t^*|^2+|\mu_t|^2b_2\right)}{|\mu_t|^2}$.

Substituting (A6) and (A7) into (A5), (20) can be obtained in Theorem 2.

The proof is completed.

References

1. Li, X.; Li, J.; Liu, Y.; Ding, Z.; Nallanathan, A. Residual Transceiver Hardware Impairments on Cooperative NOMA Networks. *IEEE Trans. Wirel. Commun.* **2020**, *19*, 680–695. [CrossRef]
2. Li, X.; Liu, M.; Deng, C.; Zhang, D.; Gao, X.C.; Rabie, K.M.; Kharel, R. Joint Effects of Residual Hardware Impairments and Channel Estimation Errors on SWIPT Assisted Cooperative NOMA Networks. *IEEE Access* **2019**, *7*, 135499–135513. [CrossRef]
3. Magueta, R.; Castanheira, D.; Silva, A.; Dinis, R.; Gameiro, A. Hybrid Multi-UserEqualizer for Massive MIMO Millimeter-WaveDynamic Subconnected Architecture. *IEEE Access* **2019**, *7*, 79017–79029. [CrossRef]
4. Ghosh, A.; Maeder, A.; Baker, M.; Chandramouli, D. 5G Evolution: A View on 5G Cellular Technology Beyond 3GPP Release 15. *IEEE Access* **2019**, *7*, 127639–127651. [CrossRef]
5. Kara, F.; Kaya, H. Threshold-Based Selective Cooperative-NOMA. *IEEE Commun. Lett.* **2019**, *23*, 1263–1266. [CrossRef]

6. Li, X.; Li, J.; Li, L. Performance Analysis of Impaired SWIPT NOMA Relaying Networks Over Imperfect Weibull Channels. *IEEE Syst. J.* **2019**, 1–4. [CrossRef]
7. Deng, C.; Zhao, X.; Zhang, D.; Li, X.; Li, J.; Cavalcante, C.C. Performance Analysis of NOMA-based Relaying Networks with Transceiver Hardware Impairments. *KSII Trans. Internet Inf. Syst.* **2018**, *12*, 4295–4316.
8. Fu, Y.; Salaün, L.; Sung, C.W.; Chen, C.S. Subcarrier and Power Allocation for the Downlink of Multicarrier NOMA Systems. *IEEE Trans. Veh. Technol.* **2018**, *67*, 11833–11847. [CrossRef]
9. Yang, Z.; Xu, W.; Pan, C.; Pan, Y.; Chen, M. On the Optimality of Power Allocation for NOMA Downlinks With Individual QoS Constraints. *IEEE Commun. Lett.* **2017**, *21*, 1649–1652. [CrossRef]
10. Ding, Z.; Dai, H.; Poor, H.V. Relay Selection for Cooperative NOMA. *IEEE Trans. Commun.* **2016**, *67*, 5084–5098. [CrossRef]
11. Ribeiro, F.C.; Dinis, R.; Cercas, F.; Silva, A. Receiver Design for the Uplink of Base Station Cooperation Systems employing SC-FDE Modulations. *EURASIP J. Wirel. Commun. Netw.* **2015**, *2015*, 1–17. [CrossRef]
12. Liau, Q.Y.; Leow, C.Y. Successive User Relaying in Cooperative NOMA System. *IEEE Wirel. Commun. Lett.* **2019**, *8*, 921–924. [CrossRef]
13. Kara, F.; Kaya,H. On the Error Performance of Cooperative-NOMA With Statistical CSIT. *IEEE Commun. Lett.* **2019**, *23*, 128–131. [CrossRef]
14. Abbasi, O.; Ebrahimi, A.; Mokari, N. NOMA Inspired Cooperative Relaying System Using an AF Relay. *IEEE Wirel. Commun. Lett.* **2019**, *8*, 261–264. [CrossRef]
15. Luo, S.; Teh, K.C. Adaptive Transmission for Cooperative NOMA System With Buffer-Aided Relaying. *IEEE Commun. Lett.* **2017**, *21*, 937–940. [CrossRef]
16. Yue, X.; Liu, Y.; Kang, S.; Nallanathan, A.; Chen, Y. Joint beamforming optimisation for NOMA-based wireless powered multi-pair two-way AF and DF relaying networks. *IEEE Trans. Commun.* **2018**, *66*, 3784–3796. [CrossRef]
17. Bae, J.; Han, Y. Joint Power and Time Allocation for Two-Way Cooperative NOMA. *IEEE Trans. Veh. Technol.* **2019**, *68*, 12443–12447. [CrossRef]
18. Zheng, B.; Wen, M.; Wang, C.; Wang, X.; Chen, F.; Tang, J.; Ji, F. Secure NOMA Based Two-Way Relay Networks Using Artificial Noise and Full Duplex. *IEEE J. Sel. Areas Commun.* **2018**, *36*, 1426–1440. [CrossRef]
19. Tang, R.; Cheng, J.; Cao, Z. Energy-Efficient Power Allocation for Cooperative NOMA Systems With IBFD-Enabled Two-Way Cognitive Transmission. *IEEE Commun. Lett.* **2019**, *23*, 1101–1104. [CrossRef]
20. Manglayev, T.; Kizilirmak, R.C.; Kho, Y.H.; Bazhayev, N.; Lebedev, I. NOMA with imperfect SIC implementation. In Proceedings of the IEEE EUROCON 2017–17th International Conference on Smart Technol, Ohrid, Macedonia, 6–8 July 2017; pp. 22–25.
21. Liu, M.; Song, T.X.; Gui, G. Deep Cognitive Perspective: Resource Allocation for NOMA-Based Heterogeneous IoT With Imperfect SIC. *IEEE Internet Things J.* **2019**, *6*, 2885–2894. [CrossRef]
22. Im, G.; Lee, J.H. Outage Probability for Cooperative NOMA Systems with Imperfect SIC in Cognitive Radio Networks. *IEEE Commun. Lett.* **2019**, *23*, 692–695. [CrossRef]
23. Mahady, I.A.; Bedeer, E.; Ikki, S.; Yanikomeroglu, H. Sum-Rate Maximization of NOMA Systems Under Imperfect Successive Interference Cancellation. *IEEE Commun. Lett.* **2019**, *23*, 474–477. [CrossRef]
24. Kolomvakis, N; Matthaiou, M.; Coldrey, M. Outage probability under I/Q imbalance and cascaded fading effects. *IEEE Trans. Commun.* **2016**, *64*, 3039–3051. [CrossRef]
25. Parikh, V.K.; Balsara, P.T.; Eliezer, O.E. All digital-quadrature-modulator based wideband wireless transmitters. *IEEE Trans. Circuits Syst.* **2009**, *56*, 2487–2497. [CrossRef]
26. Zhang, Y.P.; Li, X.J.; Phang, T.Y. A study of dual-mode bandpass filter integrated in BGA package for single-chip RF transceivers. *IEEE Trans. Adv. Packag.* **2006**, *29*, 354–358. [CrossRef]
27. Solanki, S.; Upadhyay, P.K.; da Costa, D.B.; Bithas, P.S.; Kanatas, A.G.; Dias, U.S. Joint Impact of RF Hardware Impairments and Channel Estimation Errors in Spectrum Sharing Multiple-Relay Networks. *IEEE Trans. Commun.* **2018**, *66*, 3809–3824. [CrossRef]
28. Li, X.; Liu, M.; Deng, D.; Li, J.; Deng, Ch.; Yu, Q. Power Beacon Assisted Wireless Power Cooperative Relaying using NOMA with Hardware Impairments and Imperfect CSI. *AEU - Int. J. Electron. Commun.* **2019**, *108*, 275–286. [CrossRef]
29. Teodoro, S.; Silva, A.; Dinis, R.; Barradas, F.M.; Cabral, P.M.; Gameiro, A. Theoretical Analysis of Nonlinear Amplification Effects in Massive MIMO Systems. *IEEE Access* **2019**, *7*, 172277–172289. [CrossRef]

30. Tian, X.; Li, Q.; Li, X.; Zhang, H.; Rabie, K.; Cavalcante, C.C. Performance Analysis of Two-Way Relay NOMA Systems with Hardware Impairments and Channel Estimation Errors. *Ksii Trans. Internet Inf. Syst.* **2019**, *13*, 5370–5493.
31. Li, X.; Huang, M.; Li, J.; Yu, Q.; Rabie, K.; Cavalcante, C.C. Secure Analysis of Multi-Antenna Cooperative Networks with Residual Transceiver HIs and CEEs. *IET Commun.* **2019**, *13*, 2649–2659. [CrossRef]
32. Li, X.; Liu, M.; Deng, C.; Mathiopoulos, P.T.; Ding, Z.; Liu, Y. Full-Duplex Cooperative NOMA Relaying Systems with I/Q Imbalance and Imperfect SIC. *IEEE Wirel. Commun. Lett.* **2019**, *9*, 1–1. [CrossRef]
33. Mohajeran, S.A.; Sadough, S.M.S. On the Interaction Between Joint Tx/Rx IQI and Channel Estimation Errors in DVB-T Systems. *IEEE Syst. J.* **2018**, *12*, 3271–3278. [CrossRef]
34. Kolomvakis, N.; Coldrey, M.; Eriksson, T.; Viberg, M. Massive MIMO Systems With IQ Imbalance: Channel Estimation and Sum Rate Limits. *IEEE Trans. Commun.* **2017**, *65*, 2382–2396. [CrossRef]
35. Beaulieu, N.C.; Hemachandra, K.T. Novel Representations for the Bivariate Rician Distribution. *IEEE Trans. Commun.* **2011**, *59*, 2951–2954. [CrossRef]
36. Rice, S.O. Mathematical analysis of random noise. *Bell Syst. Tech. J.* **1944**, *23*, 282–332. [CrossRef]
37. Li, J.; Matthaiou, M.; Svensson, T. I/Q Imbalance in Two-Way AF Relaying. *IEEE Trans. Commun.* **2014**, *62*, 2271–2285. [CrossRef]
38. Selim, B.; Muhaidat, S.; Sofotasios, P.C.; Sharif, B.S.; Stouraitis, T.; Karagiannidis, G.K.; Al-Dhahir, N. Performance Analysis of Non-Orthogonal Multiple Access Under I/Q Imbalance. *IEEE Access* **2018**, *6*, 18453–18468. [CrossRef]
39. Li, X.; Wang, Q.; Peng, H.; Zhang, H.; Do, D.T.; Rabie, K.; Cavalcante, C. A unified framework for HS-UAV NOMA networks: Performance analysis and location optimization. *IEEE Access* **2019**, *8*, 13329–13340. [CrossRef]